

# Improved cholesterol phenotype analysis by a model relating lipoprotein life cycle processes to particle size<sup>S</sup>

Daniël B. van Schalkwijk,<sup>1,\*†</sup> Albert A. de Graaf,<sup>\*</sup> Ben van Ommen,<sup>\*</sup> Kees van Bochove,<sup>\*</sup> Patrick C. N. Rensen,<sup>§</sup> Louis M. Havekes,<sup>\*,§</sup> Niek C. A. van de Pas,<sup>\*</sup> Huub C. J. Hoefsloot,<sup>\*\*</sup> Jan van der Greef,<sup>\*,†</sup> and Andreas P. Freidig<sup>††</sup>

TNO Quality of Life, Business Unit Biosciences,<sup>\*</sup> Zeist and Leiden, The Netherlands; Leiden Amsterdam Centre for Drug Research (LACDR), Analytical Sciences Division,<sup>†</sup> Leiden, The Netherlands; Departments of General Internal Medicine, Endocrinology and Metabolic Diseases and Cardiology,<sup>§</sup> Leiden University Medical Centre (LUMC), Leiden, The Netherlands; Biosystems Data Analysis,<sup>\*\*</sup> Swammerdam Institute for Life Sciences, University of Amsterdam, Amsterdam, The Netherlands; and Amsterdam Molecular Therapeutics (AMT),<sup>††</sup> Amsterdam, The Netherlands

**Abstract** Increased plasma cholesterol is a known risk factor for cardiovascular disease. Lipoprotein particles transport both cholesterol and triglycerides through the blood. It is thought that the size distribution of these particles codeetermines cardiovascular disease risk. New types of measurements can determine the concentration of many lipoprotein size-classes but exactly how each small class relates to disease risk is difficult to clear up. Because relating physiological process status to disease risk seems promising, we propose investigating how lipoprotein production, lipolysis, and uptake processes depend on particle size. To do this, we introduced a novel model framework (Particle Profiler) and evaluated its feasibility. The framework was tested using existing stable isotope flux data. The model framework implementation we present here reproduced the flux data and derived lipoprotein size pattern changes that corresponded to measured changes. It also sensitively indicated changes in lipoprotein metabolism between patient groups that are biologically plausible. Finally, the model was able to reproduce the cholesterol and triglyceride phenotype of known genetic diseases like familial hypercholesterolemia and familial hyperchylomicronemia. **In the future, Particle Profiler can be applied for analyzing detailed lipoprotein size profile data and deriving rates of various lipolysis and uptake processes if an independent production estimate is given.**—van Schalkwijk, D. B., A. A. de Graaf, B. van Ommen, C. van Bochove, P. C. N. Rensen, L. M. Havekes, N. C. A. van de Pas, H. C. J. Hoefsloot, J. van der Greef, and A. P. Freidig. **Improved cholesterol phenotype analysis by a model relating lipoprotein lifecycle processes to particle size.** *J. Lipid Res.* 2009. 50: 2398–2411.

**Supplementary key words** kinetics • data analysis • mathematical modeling • stable isotope flux data • lipoprotein lipase • hepatic lipase • genetic polymorphism

Total cholesterol concentration in plasma has long been known to correlate with cardiovascular disease risk. Subsequent investigations have distinguished more specific fractions of plasma cholesterol to attribute this risk to. First, LDL cholesterol was identified as a risk factor and later the size distribution within that fraction was found to be of importance [for a historical review, see Ref. (1)]. Based on these findings, an ‘atherogenic lipoprotein phenotype’ has been defined, which takes into account a particle size profile within the LDL class (2). In addition to the cholesterol-based risk factors, apolipoprotein (Apo) measurements, such as ApoB or the ApoB/ApoA-I ratio, have been found to indicate atherosclerosis risk (3–5).

Further improvements in risk assessment will primarily result from a more detailed understanding of lipoprotein physiology. To increase quantitative insight, various multi-compartmental models have been developed to analyze experiments with radioactive or stable isotope labeled lipoprotein constituents. The first models describe the fluxes of ApoB between lipoprotein fractions (6–8) with subsequent refinements allowing better data interpretation (9–15). Other models describe the fluxes of triglycerides through the lipoprotein fractions (16–20)

Abbreviations: Apo, apolipoprotein; GPIIb/IIIa, glycosylphosphatidylinositol-anchored HDL-binding protein 1; HSPG, heparan sulfate proteoglycans; IDL, intermediate density lipoprotein; LRP, low density lipoprotein receptor-related protein; SR-BI, scavenger receptor class B type I.

<sup>†</sup>To whom correspondence should be addressed.

e-mail: daan.vanschalkwijk@tno.nl

<sup>S</sup>The online version of this article (available at <http://www.jlr.org>) contains supplementary data.

*D.v.S. was funded by Biorange project SP 3.3.1 of the Netherlands Bioinformatics Centre (NBIC).*

*Manuscript received 7 July 2008 and in revised form 21 November 2008 and in re-revised form 31 March 2009 and in re-revised form 2 June 2009.*

*Published, JLR Papers in Press, June 10, 2009  
DOI 10.1194/jlr.M800354-JLR200*

or combine both ApoB and triglyceride information (21). Similar models describing other apolipoprotein kinetics have also been developed (22–26). The reported models were developed to deal with various density-based lipoprotein separation techniques. Now, new measuring techniques, such as HPLC (27) and NMR measurements (28), provide more detailed size-concentration profiles of lipoproteins and their constituents. The analysis of this data is challenging, but because earlier models were not designed for this task, new model approaches are necessary.

Here, we develop the mathematical model framework Particle Profiler. The central hypothesis of the framework is that the rate of lipoprotein production, remodeling, and uptake processes depends on the size of the lipoprotein particle. First, we show that a model implementation in the Particle Profiler model framework can reproduce published stable isotope flux data (29) and analyze them using few and physiologically relevant model parameters. The analysis results are then compared with known underlying physiology, specifically the LDL peak size according to which patients were categorized in the original paper (29). The model's ability to sensitively indicate physiological differences between these groups is also demonstrated. Finally, the potential for modeling genetic defects is illustrated by evaluating the result of changes in LPL-related lipolysis rate and ApoB-related uptake rate. We discuss the framework's potential to derive lipoprotein lipolysis and uptake rate information from detailed lipoprotein size measurements and an independent production estimate.

## MODEL DEVELOPMENT

### Model framework

The lifecycle of lipoprotein particles consists of three processes: production, remodeling, and uptake. The Particle Profiler model framework starts from the assumption that the rate of each of these processes depends on the size of the lipoprotein particles. Different hypotheses about how these processes depend on particle size can lead to different model instances within the framework.

The Particle Profiler model framework is shown schematically in **Figs. 1, 2, and 3**. The particles in the Particle Profiler model are subdivided into many very small subclasses according to their size. We refer to “subclasses” for the small size ranges the model uses and to a particle size “class” for the larger size ranges that are measured in experiments, like “LDL”, “VLDL1”, etc. Figure 1 shows the processes that act on each subclass, Fig. 2 shows the particle size range of the subclasses after subsequent lipolysis steps and finally, Fig. 3 shows how the step size due to lipolysis is calculated. Mass balances can be written for each of the subclasses, and also for the sum of all subclasses in any particle size range. These equate what comes in from the lipolysis and direct production with what leaves through lipolysis and direct uptake. The equations in each subclass obey zero-

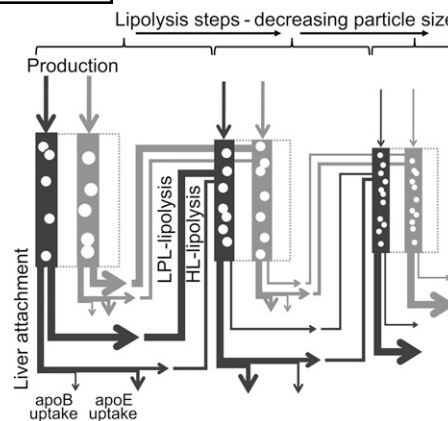


**Fig. 1.** A schematic overview of the model framework. Particles are contained in very many subclasses, each representing a narrow size range. Processes affecting the particle concentration in a subclass are production, extrahepatic lipolysis by LPL, and liver attachment. Liver attachment can in turn be followed by either hepatic lipolysis through HL, or uptake through ApoB- or ApoE-related mechanisms. If the particle is lipolyzed, it proceeds to the next step in the lipolysis cascade, which is explained in more detail in Figs. 2 and 3. Subsequent subclasses in the lipolysis cascade are smaller; that is, they generally cover a smaller size range of lipoproteins (see Fig. 2). The different thicknesses of the arrows indicate that processes have different importance at each particle size. The particle production flux is an input to the model, whereas the model adjusts the lipolysis and uptake processes to fit the data. The rates of the lipolysis and uptake processes vary continuously with particle size, as shown in the supplementary data.

order kinetics for production and first-order kinetics for all the other processes. The pool size in each subclass can therefore be solved from a linear equation. The model framework contains the new concept that rate constants of processes in different subclasses vary nonlinearly as a function of particle diameter. The parameters of these nonlinear functions can be estimated by comparing experimental data on particle concentrations and fluxes in lipoprotein size classes to the model prediction for those size classes.

The size-dependent models for production, lipolysis, and uptake are based on biological hypotheses explained below. These hypotheses were translated into mathematical equations to generate a first model instance. The current model, described below, can be considered a first functional implementation to which further biological knowledge can be added in order to arrive at new, more detailed, model instances. Each process's biology, conceptual model, and mathematical model are discussed consecutively. A full motivation of all equations can be found in the supplementary data.

### Model input

**Production. BIOLOGY.** Hepatic production of VLDL particles (30) is thought to be a two-step process. First, VLDL2 is produced intracellularly through a first lipidation of an ApoB100 molecule. VLDL2 can then be fused to a lipid droplet to form VLDL1 (31). LDL and intermediate density lipoprotein (IDL) are, for the greatest part, lipolytic products of the VLDL particles. Whether a small fraction

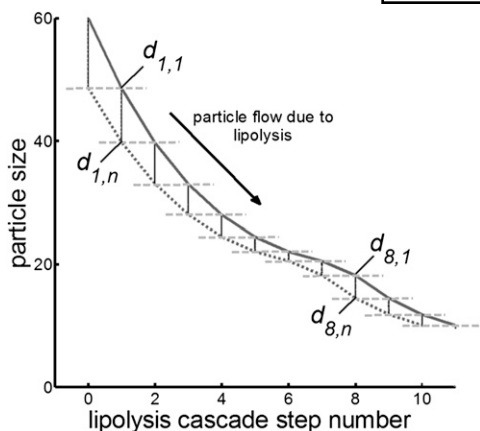


**Fig. 2.** The particle size range (in nm) of the subclasses after subsequent lipolysis cascade steps. Each particle size range of a given lipolysis cascade step, indicated by a black bar in the figure, is subdivided into  $n$  subclasses, in the current implementation  $n$  equals 1149, corresponding to a maximum interval of 0.01 nm per subclass. Particles can be produced at all sizes ranging from approximately 14–60 nm. If a particle is lipolyzed, it will always flow into a subclass in the size range (Y-axis) of the next cascade step (X-axis). A particle that is produced in a given subclass with particle size  $d_{i,j}$  ( $i$ , cascade step number,  $j$ , subclass number within cascade step) will always flow into a subsequent subclass with particle size  $d_{i+1,j}$ . This is because the particle changes its size deterministically and always loses a fixed percentage of triglycerides at each lipolysis step as illustrated in Fig. 3. The solid and dotted gray lines in this figure indicate two routes that a particle may take as it is lipolyzed, one at the top ( $d_{i,1}$ ) and another at the bottom ( $d_{i,n}$ ) of the lipolysis step size ranges. The particle size ranges of subsequent lipolysis steps do not overlap.

of these lipoproteins is produced directly is still a matter of debate. Stable isotope flux studies generally show a small amount of direct input into these classes.

**CONCEPTUAL MODEL.** The current production model contains four size classes (VLDL1, VLDL2, IDL, and LDL), and specifies how the influx into these large classes is distributed over many subclasses, which each have a narrow size range. The total production flux into each large class is based directly on the lipoprotein flux data of each subject (29).

The expected biological variation in the amount of lipids added to ApoB during the production process makes it very unlikely that production falls in one very narrow size range. The size of VLDL 2 particles is expected to vary around a given mean, because its size is based on the structure of ApoB plus a first lipidation (32). We therefore assume that the diameter of secreted VLDL2 particles is normally distributed within the VLDL2 range. In the case of VLDL1, the size of the fused lipid droplets in the second production step can vary greatly (33). Therefore, we used a lognormal size distribution in the VLDL1 range, which allows the incidental production of larger particles in its ‘tail’. Inasmuch as the IDL and LDL production processes are under debate, a normal size distribution within these classes was thought to be the best option.

**MATHEMATICAL MODEL.** The production flux into the LDL class can be discretized as follows:

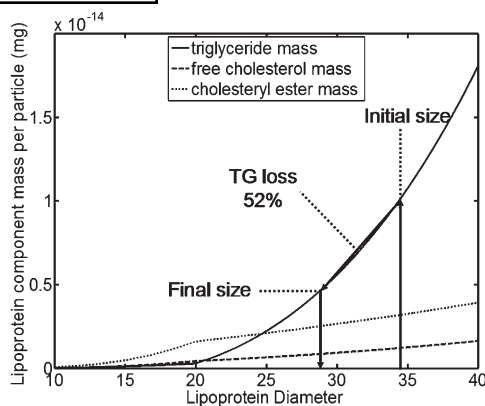


**Fig. 3.** Calculation of change in lipoprotein particle diameter due to a percentage change in triglyceride content. The model calculation proceeds in three steps. First, the model calculates the triglyceride content of the particle at its initial size. Second, it calculates the final triglyceride content after lipolysis during which the particle loses 52% of its triglycerides. Third, it calculates the particle size corresponding to the calculated final triglyceride content, which is the particle size after lipolysis. The relation between lipoprotein diameter and composition was based on the model presented by Tuzikov et al. (34). Solid line, triglyceride mass per particle; striped line, free cholesterol mass per particle; dotted line, cholesteryl ester mass per particle.

$$J_p(d_{i,j}) = \frac{J_{p,LDL} * \left( \Phi_{d_{LDL},\sigma} \left( d_{i,j} + \frac{1}{2} d_{i,j}^r \right) - \Phi_{d_{LDL},\sigma} \left( d_{i,j} - \frac{1}{2} d_{i,j}^r \right) \right)}{\Phi_{d_{LDL},\sigma} (d_{LDL,max}) - \Phi_{d_{LDL},\sigma} (d_{LDL,min})}$$

for

$$d_{i,j} + \frac{1}{2} d_{i,j}^r \leq d_{LDL,max}$$

$$d_{i,j} - \frac{1}{2} d_{i,j}^r \geq d_{LDL,min}$$

(eq.1)

In this equation,  $J_p(d_{i,j})$  is the influx due to production into a subclass with average particle diameter  $d_{i,j}$ , and subclass resolution  $d_{i,j}^r$ . The subindices refer to the lipolysis step ( $i$ ) and the subclass within that lipolysis step range ( $j$ ) (see Fig. 2). These subclasses have a variable resolution, which is always smaller than 0.01nm in the current implementation.  $J_{p,LDL}$  is the production rate in the LDL class, which is fixed based on the production data of each subject (29) (see **Table 1**).  $\Phi$  is the Gaussian cumulative density function,  $d_{LDL}$  stands for the mean diameter of the LDL class,  $\sigma$  is the standard deviation of the distribution curve, and subscripts indicate the class to which a diameter refers and whether it is a minimum or maximum value for that class. In the lower boundary subclass, which lies only partially in the LDL class,  $(d_{i,j} - \frac{1}{2} d_{i,j}^r)$  is replaced by the lower border of the LDL class,  $d_{LDL,min}$ ; in the upper boundary subclass,  $(d_{i,j} + \frac{1}{2} d_{i,j}^r)$  is replaced by the upper border of the LDL class,  $d_{LDL,max}$ . For the IDL and VLDL2 classes, the production is defined analogously.

For the VLDL1 class, the normal distribution is replaced by the lognormal distribution as follows:

TABLE 1. Overview of state variables, variables, parameters, and constants used in this model

State Variables—Determine the System State		
$d_{i,j}$	nm	Lipoprotein particle diameter in the $i$ -th step of a lipolysis cascade, in the $j$ -th subclass of the size range covered by that cascade step
$Q_{ss}(d_{i,j})$	Particles * $d_l^{-1}$	Steady-state particle pool size in a pool with mean particle diameter $d_{i,j}$
Variables – specify processes and output		
$J_p(d_{i,j})$	Particles * $d_l^{-1}$ * $day^{-1}$	Particle production flux into the pool with mean particle diameter $d_{i,j}$
$J_l(d_{i,j})$	Particles * $d_l^{-1}$ * $day^{-1}$	Particle flux into the pool with mean particle diameter $d_{i,j}$ due to extrahepatic lipolysis
$J_{l,liver}(d_{i,j})$	Particles * $d_l^{-1}$ * $day^{-1}$	Particle flux into the pool with mean particle diameter $d_{i,j}$ due to hepatic lipolysis
$k_l(d)$	$day^{-1}$	Particle size dependent extrahepatic lipolysis rate
$k_{a,liver}(d)$	$day^{-1}$	Particle size dependent liver attachment rate (attachment is followed by either lipolysis or uptake)
$k_{l,liver}(d)$	$day^{-1}$	Particle size dependent liver lipolysis rate
$k_{u,liver}(d)$	$day^{-1}$	Particle size dependent liver uptake rate
$n_{tg}(d_{i,j})$	Molecules * particle $^{-1}$	Number of triglyceride molecules in a lipoprotein particle with diameter $d_{i,j}$
$Q_{out}(d_a, d_b)$	Particles * $d_l^{-1}$	Steady state particle pool size in interval from $d_a$ to $d_b$ in the final particle concentration profile.
Parameters – are optimized using data		
$k_{l,max}$	$day^{-1}$	maximum rate at which extrahepatic lipolysis takes place
$k_{a,apoE,max}$	$day^{-1}$	maximum rate at which liver binding mediated by ApoE takes place
$d_{a,apoE,min}$	nm	minimum particle diameter at which liver binding mediated by ApoE takes place
$k_{a,apoB}$	$day^{-1}$	rate at which liver binding mediated by ApoB takes place
$\sigma_{a,apoE}$	nm	shape parameter for liver binding mediated by ApoE
$\sigma_{u,liver}$	nm	shape parameter describing fraction of liver attachment which is taken up (instead of lipolyzed) - with changing particle size
Reparametrization – used for better data fitting (see additional material)		
$d_{a,apoE,min}$	nm	minimum particle diameter at which liver binding mediated by ApoE takes place
$k_{a,apoB}$	$day^{-1}$	rate at which liver binding mediated by ApoB takes place
$k_{30}$	$day^{-1}$	the sum of all lipolysis and uptake rates at a particle diameter of 30 nm. Definition: $k_{30} = k_{a,liver}(30) + k_l(30)$
$k_{40}$	$day^{-1}$	the sum of all lipolysis and uptake rates at a particle diameter of 40 nm
$f_{u,30}$	—	the fraction of the total lipolysis and uptake rate at a particle diameter of 30 nm that is taken up
$f_{u,40}$	—	the fraction of the total lipolysis and uptake rate at a particle diameter of 40 nm that is taken up
Model constants and derived variables – are fixed or derived from the above		
$d_{l,min}$	30 nm	minimum size at which extrahepatic lipolysis occurs
$\sigma_l$	15 nm	shape constant for extrahepatic lipolysis
$f_{tg}$	0.52	fraction of triglycerides lost with each lipolysis step (see additional material for further analysis)
$d_{VLDL1}$	41.87 nm	Mean VLDL1 particle size at production
$d_{VLDL2}$	33.54 nm	Mean VLDL2 particle size at production
$d_{IDL}$	27.5 nm	Mean IDL particle size at production
$d_{LDL}$	$\frac{25 + d_{LDL,min}}{2}$ nm	Mean LDL particle size at production
$d_{LDL,min}$	nm	Minimum particle diameter in LDL class (one lipolysis step smaller than the smallest possible lipolysis binding size $d_{a,apoE,min}$ )
$\sigma_{VLDL1}$	2.94 nm	Standard deviation of VLDL1 particle size at production
$\sigma_{VLDL2}$	1.77 nm	Standard deviation of VLDL2 particle size at production
$\sigma_{IDL}$	1.25 nm	Standard deviation of IDL particle size at production
$\sigma_{LDL}$	$\frac{d_{LDL} - d_{LDL,min}}{2}$ nm	Standard deviation of LDL particle size at production



$$J_p(d_{ij}) = \frac{J_{p,VLDL1} * \left( F_{\mu_{VLDL1}, \sigma_{in}} \left( d_{ij} + \frac{1}{2} d_{ij}^r \right) - F_{\mu_{VLDL1}, \sigma_{in}} \left( d_{ij} - \frac{1}{2} d_{ij}^r \right) \right)}{F_{\mu_{VLDL1}, \sigma_{in}}(d_{VLDL1max}) - F_{\mu_{VLDL1}, \sigma_{in}}(d_{VLDL1min})}$$

for

$$d_{ij} + \frac{1}{2} d_{ij}^r \leq d_{VLDL1max}$$

$$d_{ij} - \frac{1}{2} d_{ij}^r \geq d_{VLDL1min}$$

(eq. 2)

In this equation, F is the lognormal cumulative density function starting at  $d = d_{VLDL1min}$  with mean  $\mu_{VLDL1}$ . In the lower boundary subclass, which lies only partially in the VLDL1 range,  $(d_{ij} - \frac{1}{2} d_{ij}^r)$  is replaced by  $d_{VLDL1min}$ ; in the upper boundary subclass  $(d_{ij} + \frac{1}{2} d_{ij}^r)$  is replaced by  $d_{VLDL1max}$ .

The formula for translating the expectation  $\bar{d}_{VLDL1}$  and standard deviation  $\sigma_{VLDL1}$  for the particle diameter in the VLDL 1 class to the mean ( $\mu$ ) and standard deviation ( $\sigma_{in}$ ) of a lognormal distribution is given by:

$$\mu_{VLDL1} = \ln \left( \bar{d}_{VLDL1} - d_{VLDL1min} \right) - \frac{1}{2} \ln \left( 1 + \frac{\sigma_{VLDL1}^2}{(\bar{d}_{VLDL1} - d_{VLDL1min})^2} \right)$$

$$\sigma_{in}^2 = \ln \left( 1 + \frac{\sigma_{VLDL1}^2}{(\bar{d}_{VLDL1} - d_{VLDL1min})^2} \right)$$

(eq. 3)

Values for  $\bar{d}$  and  $\sigma_{in}$  in the various production classes can be found in Table 1. The mean size of the VLDL2 and VLDL1 classes were derived by comparing the triglyceride (TG) to ApoB ratio of the production in these classes presented by Adiels et al. (21) to the TG-particle size relation given by Tuzikov et al. (34). Because no data for IDL and LDL are available, the class middle was taken as distribution mean. The standard deviation of the curves was taken as half the distance from the distribution mean to the lower class border.

### Model optimization

*Extrahepatic tissue - lipolysis and remodeling. BIOLOGY.* In extrahepatic tissues, VLDL particles are only remodeled; uptake of whole particles is negligible (35). During remodeling, changes occur in triglyceride content as well as changes in phospholipid, cholesteryl ester, and protein composition. Changes in triglyceride content occur through lipolysis. Lipolysis of lipoproteins in extrahepatic tissues is carried out mainly by LPL. This enzyme mainly lipolyzes larger lipoproteins such as VLDL1 whereas VLDL2 and IDL are lipolyzed to a subsequently lesser extent (36). The particle binds to cell-surface heparan sulfate proteoglycans (HSPGs) and GPI-anchored HDL-binding protein 1 (GPIHBP1) (37) mainly through LPL itself whereas ApoE modulates the binding affinity (38). Multiple LPLs that are already

bound to the HSPGs can then be transferred to the lipoprotein and mediate the lipolysis of the particle. What exactly determines the rate of this lipolysis is not known, although the available surface area, the biochemical composition of the particle (39), gene expression changes, activators (e.g., ApoCII, ApoE, ApoAV), inhibitors (e.g., ApoCI, ApoCIII, Angptl4), and modulators of LPL expression (e.g., VLDL receptor) (40) are all thought to influence this rate.

*CONCEPTUAL MODEL.* Because the primary physiological function of lipoproteins is lipid transport, the current model implementation assumes that the rate of remodeling is determined by the lipolysis rate. Therefore, in this model, changes in cholesterol, phospholipid, and protein content are determined by changes in triglyceride content. Therefore, only lipolysis is explicitly modeled and so, in continuation, we will speak about "lipolysis" instead of "remodeling". In the model framework, the lipolysis process is split into two steps: the first step describes whether a particle is bound to a HSPG for lipolysis, the second, how many triglycerides it loses during lipolysis. The first step depends on the particle's binding affinity to HSPGs and GPIHBP1, which in turn depends on its apolipoprotein composition. The apolipoprotein composition is not modeled explicitly but implicitly by a function relating lipolysis rate to particle size. This means that the total affinity of the particle for HSPG increases with particle size until a maximum is reached. Once a particle is selected for lipolysis, it proceeds to the next step in the lipolysis cascade. The calculation of lipolysis cascades is described below under "Model calculation - Lipolysis cascades".

*MATHEMATICAL MODEL.* To describe the size-dependency of extrahepatic lipolysis, a cumulative density function of the Rayleigh distribution was chosen. The formula for the lipolysis binding rate in extrahepatic tissue  $k_1(d)$  (unit:  $\text{day}^{-1}$ ) then becomes:

$$k_1(d) = \begin{cases} k_{max} \left( 1 - \exp \left( -\frac{(d - d_{lmin})^2}{2\sigma_1^2} \right) \right) & \text{for } d \geq d_{lmin} \\ 0 & \text{for } d < d_{lmin} \end{cases}$$

(eq. 4)

where  $d$  is the particle diameter,  $d_{lmin}$  is the minimum size at which lipolysis occurs,  $k_{lmax}$  is the maximum lipolysis binding rate, and  $\sigma_1$  is a shape constant for describing how the lipolysis rate depends on particle size (see Table 1).

*Liver - lipolysis and uptake. BIOLOGY.* In the liver, VLDL and IDL particles first bind to liver HSPG via ApoE, whereas LDL binds directly to LDL receptors via ApoB100. LDL particles are directly taken up, but ApoE-mediated binding of larger particles need not result in uptake and can lead to lipolysis instead. The lipolysis in the liver is primarily mediated by HL, an enzyme that functions primarily on smaller ApoB- and ApoE-containing lipoproteins such as IDL, and to a lesser extent on VLDL2 (41). Uptake of VLDL lipoproteins mainly takes place via the LDL receptor but can also take place via low density lipoprotein receptor-related protein (LRP) (42). Roles for scavenger

receptor class B type I (SR-BI) and direct incorporation via HSPGs have also been suggested (43, 44).

**CONCEPTUAL MODEL.** In the model, liver binding and further processing are described as a two-step process. First, binding takes place, mainly mediated by ApoE, but with a small contribution from ApoB. Although small, this contribution is important, especially in the LDL size range where a small uptake affinity combined with large amounts of particles can result in a considerable uptake flux. Subsequently, the part of the lipoproteins bound via ApoB is taken up. The part bound through ApoE can result in either lipolysis or uptake. Here, the lipolyzed part is mainly processed by HL and because HL mainly lipolyzes smaller particles, the lipolysis/uptake ratio decreases with increasing particle size.

**MATHEMATICAL MODEL.** Because binding first increases and can subsequently decrease with particle size, a Rayleigh probability density function is used to describe this pattern. In order to have its maximum at one, it is scaled using the maximum of this same function, which lies at  $d = \sigma_{a,apoE}$ .

$$k_{a,liver}(d) = \begin{cases} k_{a,apoEmax} \left( \frac{(d - d_{a,apoEmin}) \exp\left(-\frac{(d - d_{a,apoEmin})^2}{2(\sigma_{a,apoE} - d_{a,apoEmin})^2}\right)}{(\sigma_{a,apoE} - d_{a,apoEmin}) \exp\left(\frac{-1}{2}\right)} \right) & \text{for } d \geq d_{a,apoEmin} \\ +k_{a,apoB} & \text{for } d \geq d_{a,apoEmin} \\ k_{a,apoB} & \text{for } d < d_{a,apoEmin} \end{cases} \quad (eq. 5)$$

The resulting liver uptake function is given by:

$$k_{u,liver}(d) = \begin{cases} (k_{a,liver} - k_{a,apoB}) \left( 1 - \exp\left(-\frac{(d - d_{a,apoEmin})^2}{2\sigma_{u,liver}^2}\right) \right) & \text{for } d \geq d_{a,apoEmin} \\ +k_{a,apoB} & \text{for } d \geq d_{a,apoEmin} \\ k_{a,apoB} & \text{for } d < d_{a,apoEmin} \end{cases} \quad (eq. 6)$$

Because binding to the liver can result in either uptake or lipolysis (see conceptual model above), lipolysis in the liver is given by:

$$k_{l,liver}(d) = k_{a,liver}(d) - k_{u,liver}(d) \quad (eq. 7)$$

The model for these liver processes does not include a separate pool of attached particles. The model, rather, considers that attachment is directly followed by either uptake or lipolysis.

### Model calculation

**Lipolysis cascades. BIOLOGY.** ApoB-containing lipoproteins go through a sequence of delipidation steps during which they become successively smaller. The lipoprotein particle that has been bound to the vascular wall is lipolyzed extrahepatically mainly by LPL (45) and, in the liver, mainly by

HL (46). The resulting flux of particles from size classes with larger particles to size classes with smaller particles has often been measured using stable isotope and radioactive tracer techniques. In vitro free fatty acid release from VLDL through LPL has been found to be related to triglyceride-ApoB ratios (47) and triglyceride-cholesterol ratios (48). However, exactly how large a step the lipoprotein particles make per lipolysis event cannot be measured in vivo.

**CONCEPTUAL MODEL.** A particle is produced with a certain diameter and can go through a variable number of lipolysis steps before being taken up. Figure 2 shows how the size of a particle decreases as the particle goes through subsequent lipolysis steps. Each lipolysis step has a corresponding size range, which generally becomes smaller as the particles are smaller. A lipolysis step size range is always divided into the same number of subclasses, 1149 in the current implementation (0.01 nm resolution at the crudest). This arrangement makes it possible for all particles that are produced in a particular subclass to flow through to the same subsequent subclass in the lipolysis cascade. In this way, the concentration in each particle size range can be calculated efficiently.

For calculating a particle's size reduction due to lipolysis, we tested two alternative models. Both models first calculate the particle's triglyceride content but differ in the subsequent calculations. The first model takes out a fixed quantity of triglyceride molecules, the second takes out a fixed percentage of triglycerides from the particle as is shown in Fig. 3. Finally, the model calculates the final particle size from the amount of triglyceride molecules that remain.

The model version that assumes the loss of a fixed quantity of triglyceride molecules per lipolysis step proved to be unable to fit the flux data (model fits not shown). Therefore, we opted for the model version that assumes the particle loses a fixed percentage of triglycerides per lipolysis step. This option fits well with the importance of the triglyceride-ApoB and triglyceride-cholesterol ratio for enzyme activity observed in vitro (47, 48) because larger particles that contain more triglycerides also lose more triglycerides. Alternatives are possible such as the stochastic step-size model Adiels (39) presented. However, with the current model and the dataset we consider here, we cannot discriminate between the simpler mechanism with a fixed step size and a more complicated mechanism with a stochastic step size. We have therefore chosen the simplest model that can reproduce the data, in which a particle loses a fixed percentage of triglycerides per lipolysis step.

**MATHEMATICAL MODEL.** The relation between particle diameter and both particle cholesterol and triglyceride content was based on an empirical model presented by Tuzikov et al. (34) shown in Fig. 3. This model is a combination of two exponential functions fitted to literature and newly measured data on the percentage composition of lipoproteins at different particle sizes. Although it is known that particles of a given size do not always have the same biochemical composition, the current approach gives a first

approximation, which may still be improved in future versions of the model.

The change in particle diameter through lipolysis is calculated as follows. Particle diameters are denoted by  $d_{i,j}$  where the particle's cascade step (see Fig. 2) is indicated with index  $i$  and the subclass within that cascade step is indicated with index  $j$ . The size change due to the cascade step from  $d_{i,j}$  to  $d_{i+1,j}$  is determined by a model parameter specifying the triglyceride fraction a particle loses during lipolysis ( $f_{ig}$ ). The equation for the loss of triglycerides is given by:

$$n_{ig}(d_{i+1,j}) = (1 - f_{ig})n_{ig}(d_{i,j}) \quad (eq. 8)$$

where  $n_{ig}(d_{i,j})$  is the initial and  $n_{ig}(d_{i+1,j})$  the final number of triglyceride molecules in a lipoprotein particle, as a function of particle diameter.

**Particle concentrations in cascade. CONCEPTUAL MODEL.** Particles are produced in many small subclasses. In the subclasses containing very large particles, the only particle influx is due to production but, in subclasses containing smaller particles, there is an additional influx due to the lipolysis process. This is shown schematically in Fig. 1. A steady-state particle pool is calculated in each subclass by dividing the total particle influx (particles/s) due to either production or lipolysis by the total efflux rate (1/s) due to lipolysis and uptake. This calculation proceeds from the mass balance in each subclass at steady state. In this way, the particle concentration in each small subclass can be calculated efficiently using the steady-state assumption.

The resolution of the subclasses becomes smaller as particle size becomes smaller. This is because particles that are produced in the same subclass all proceed through the same sequence of subclasses as they are lipolyzed (see Figs. 1, 2). The initial size difference of the large particles within one subclass is slowly mitigated through the lipolysis process.

**MATHEMATICAL MODEL.** The steady-state pool  $Q_{ss}(d_{i,j})$  at each mean subclass particle diameter  $d_{i,j}$  is given by:

$$Q_{ss}(d_{i,j}) = \frac{J_p(d_{i,j}) + J_l(d_{i,j}) + J_{l,liver}(d_{i,j})}{k_l(d_{i,j}) + k_{l,liver}(d_{i,j}) + k_{u,liver}(d_{i,j})} \quad (eq. 9)$$

where  $J_p(d_{i,j})$  is the particle influx resulting from production,  $J_l(d_{i,j})$  is the particle influx resulting from extrahepatic lipolysis,  $J_{l,liver}(d_{i,j})$  is the particle influx resulting from hepatic lipolysis,  $k_l$  is the extrahepatic lipolysis rate,  $k_{l,liver}$  is the hepatic lipolysis rate and  $k_{u,liver}$  is the particle uptake rate. These influxes due to lipolysis are calculated iteratively as follows:

$$\begin{aligned} J_l(d_{i,j}) &= k_l(d_{i-1,j}) \times Q_{ss}(d_{i-1,j}) \\ J_{l,liver}(d_{i,j}) &= k_{l,liver}(d_{i-1,j}) \times Q_{ss}(d_{i-1,j}) \end{aligned} \quad (eq. 10)$$

The influx due to production  $J_p(d_{i,j})$  is given in equations 1 and 2.

## Model output

**Particle profile. CONCEPTUAL MODEL.** The model calculates a detailed size-concentration lipoprotein profile with the resolution that was used for calculation; in this study, a 0.01 nm resolution was used. This profile can be shown as such or as size classes that correspond to experimental measurements. Examples of other possible output classes include the classical VLDL1, VLDL2, IDL, and LDL classes and size classes measured by HPLC (27) or NMR (28) techniques. The model output in the first instance includes steady-state particle concentrations but can also show steady-state fluxes of production, lipolysis, and uptake at each particle size.

**MATHEMATICAL MODEL.** The equation for the total steady-state output pool  $Q_{out}$  in a given diameter range  $[d_a, d_b]$  is given by:

$$Q_{out}([d_a, d_b]) = \sum_{\substack{d_{i,j} + \frac{1}{2}d_{ij}^r \leq d_b \\ d_{i,j} - \frac{1}{2}d_{ij}^r \geq d_a}} Q_{ss}(d_{i,j}) + R \quad (eq. 11)$$

where  $Q_{ss}(d_{i,j})$  is the steady-state pool calculated in the model at diameter  $d_{i,j}$ .  $R$  is the remainder for the boundary subclasses, which partially fall in the selected range:

$$\begin{aligned} R_{low} &= \frac{\left(d_{i,j} + \frac{1}{2}d_{ij}^r\right) - d_a}{d_{i,j}^r} Q_{ss}(d_{i,j}) \quad \text{where } d_a \in [d_{i,j} - \frac{1}{2}d_{ij}^r, d_{i,j} + \frac{1}{2}d_{ij}^r] \\ R_{high} &= \frac{d_b - \left(d_{i,j} - \frac{1}{2}d_{ij}^r\right)}{d_{i,j}^r} Q_{ss}(d_{i,j}) \quad \text{where } d_b \in [d_{i,j} - \frac{1}{2}d_{ij}^r, d_{i,j} + \frac{1}{2}d_{ij}^r] \\ R &= R_{high} + R_{low} \end{aligned} \quad (eq. 11a)$$

**Triglyceride and cholesterol concentrations.** The particle profiles are translated to triglyceride and cholesterol profiles by the same size-composition relation used above to calculate the lipolysis cascades. It uses an empirical model presented by Tuzikov et al. (34) shown in Fig. 3.

## Model implementation

The model was implemented in MATLAB version 7.5.0(R2007b).

## Model testing

**Data used.** In order to test the model's capability to reproduce measured lipoprotein flux data, the model was fitted to flux data preanalyzed by a multi-compartment model from a stable isotope labeling study by Packard et al. (29). Packard and coworkers divided their subjects into three groups based on the 'LDL peak size'. Phenotype A had an LDL peak size greater than 26 nm; phenotype I, an LDL peak size between 25 and 26 nm; and phenotype B, an LDL peak size smaller than 25 nm.

Packard et al. (29) analyzed the ApoB flux data of each subject by a multi-compartment model. This yielded the pool size of each lipoprotein density fraction, the influx



from the previous class into the reported class, here interpreted as the lipolysis flux, and the direct catabolism from the fraction, here presented as uptake. Also, the direct production into each class was quantified. Production fluxes were used as input to our model whereas the pool sizes (4 data points), lipolysis fluxes (3 data points), and uptake fluxes (4 data points) were fitted using six parameters (see Table 1).

The reported dataset of a subject was considered to be suitable as input to our model if it passed a “steady-state” test. The total influx should equal the total efflux in each class of the dataset. Datasets with a large imbalance (influx-efflux difference >10%) in one class were disregarded, leading to the exclusion of four patients (numbers 10, 13, 15, and 16). This selection is necessary because the current model assumes steady state, which therefore needs to be present in the data.

Because the original paper separated the VLDL1, VLDL2, IDL, and LDL categories, the model was adapted to reproduce these size classes as specified under “size classes” in the supplementary data.

*Fitted parameters.* The parameters as arising from the equations above (see Table 1) were found to be correlated with respect to the used dataset. A parameter set was designed in which correlations were kept to a minimum, which is shown under reparametrization in Table 1. The definitions can be found in the supplementary data.

The datasets used here to fit our model parameters do not contain enough information to estimate the values of all unknowns. We therefore estimated two constants related to the particle-size dependence of extrahepatic lipolysis,  $d_{\min}$  and  $\sigma$ , as shown in Table 1. We also fixed the value for the triglyceride loss per lipolysis step ( $f_{\text{ig}}$ ) at 0.52, a 52% triglyceride loss per lipolysis step. We fitted all patients with a range of values for  $f_{\text{ig}}$  and 0.52 fitted best overall (analysis not shown). Other model parameters showed a limited covariation with this choice as shown for one patient in the supplementary data.

*Fitting routine.* Parameters were fitted to the data using MATLAB's `nlinfit` method of version 7.5.0 (R2007b), which is an implementation of the Levenberg-Marquardt algorithm. The supplementary data shows the error function used.

Because we are fitting six parameters to 11 data points, there is a real possibility of finding multiple optima in the parameter landscape. We maximized the security of finding the global optimum by first scanning the parameter space for good initial conditions and subsequently starting the algorithm from multiple starting points. The parameter space was scanned by applying a full ‘experimental design’ on estimates of the upper and lower bound of each parameter. The model was evaluated at each of these 64 points. We then evaluated the middle points in parameter space between six points with the lowest error values. In total, this results in 79 model evaluations. Of these 79, we used 12 with the lowest error value as starting points for the fitting routine. After one fitting round, the six best fits

were selected as input to a new fitting round; of these outcomes, then, the three best were selected for a final fitting round. The three final parameter sets were then compared. If the final parameters were found to differ, the whole procedure was repeated using the minima and maxima of each parameter in the set of final parameters as starting points for a new experimental design. If the difference was negligible (parameter difference <1%), the best fitting parameter set was chosen.

*Statistics.* Differences in fitted parameters between the groups defined by Packard et al. (29) were inspected using the nonparametric Kruskal-Wallis test as implemented in MATLAB.

*Output parameters.* To improve interpretation, we derived various process-indicating parameters from the fitted model parameters. A first group contains process indicators, such as the maximum HL activity, the particle size at which it HL affinity is at a maximum, and the average ApoE-related uptake affinity over the VLDL1 range. A second group contains size-class specific indicator parameters of process, age, or size averages per particle in that class. For example, the average lipolysis binding rate per particle in the VLDL1 size class was calculated. This is an improvement over the ‘transfer from VLDL1 to VLDL2’ variable presented by Packard and coworkers, because it takes into account all lipolysis steps of VLDL1 particles, including those that do not cause the particle to change class.

*Simulation of defects.* Finally, the model's potential for modeling biological defects was investigated. Two defects were simulated. The first is a polymorphism in the ApoB-related uptake, which leads to hypercholesterolemia, the second a defect in LPL lipolysis, which leads to hypertriglyceridemia. Data from Patient 20 in Packard et al. (29) was chosen for the in-silico experiment because this patient has both a substantial amount of LPL lipolysis and ApoB-related uptake. The patient is in the B category with low LDL peak size and higher cardiovascular disease risk. The profile of the patient was first compared with a situation in which the ApoB-related uptake activity was halved, corresponding to a heterozygous LDL-receptor deficiency (familial hypercholesterolemia). This was simulated by setting the  $k_{a,\text{apoB}}$  parameter to half its original value. Second, the LPL-mediated lipolysis activity was reduced, corresponding to an LPL defect. This was simulated by setting the  $k_{\text{lmax}}$  value to 50% of its original value. The output of the model is reproduced for the LDL, IDL, VLDL1, and VLDL2 size classes.

## RESULTS

### Feasibility of model approach

The pool and flux data were well fitted with the Particle Profiler model. In all patients, the model fit converged to a difference of less than 1% between parameters in the



three best fit parameter sets. The minimum with the smallest error value was chosen. **Table 2** shows the parameters that have been estimated for all subjects from the study by Packard et al. and the corresponding deviations, the definition of which can be found in the supplementary data. The deviation ranged from 1.6% to 16.6% with an average of 7.2%. Only patients 4, 8, and 18 have a deviation above 10%. It is striking that these patients have high particle uptake from both the LDL and VLDL1 classes but low to very low uptake from the intermediate IDL and VLDL2 classes. The current model was not able to reproduce this pattern. Therefore, our model could reproduce the flux data of 13 out of 16 patients accurately.

### Prediction of LDL size shift

With Particle Profiler, we simulated detailed particle size profiles, although the model was fitted to pools and fluxes of only four density categories (VLDL 1, VLDL 2, IDL, and LDL). These detailed profiles were averaged for all patients in each phenotype class defined by Packard et al. In **Fig. 4**, these averaged profiles are shown. Although the A and I category profiles overlap, a shift toward lower LDL sizes was observed as the phenotype changes from A and I to B, corresponding to the size shift measured by Packard. This result points to the physiological realism of the model because, with no size data other than an estima-

tion of the particle size ranges of each density class, the model still qualitatively reproduced an LDL particle size shift.

The particle size shift was also visible in the model parameters. The parameter most directly associated to this shift is the lipolysis minimum size, because, if small particles are lipolyzed more, they will become even smaller. The value of this parameter seems realistic for all patients except possibly patient 19, where the lipolysis minimum size hits the minimum boundary of 11 nm. The Kruskal-Wallis test showed that the median of the lipolysis minimum size significantly decreased from group A and I to group B, with  $P = 0.014$ . This shows that both the modeled size-concentration profiles and the model parameters qualitatively reproduced the LDL size shift between the groups.

### Process identification

**Table 3** shows the derived parameters that indicate the status of the various physiological processes. Next to the lipolysis minimum size, the HL peak binding rate and the ApoB-related uptake rate also have significantly different medians between the groups.

**Table 4** shows the size-class specific indicator parameters with a significantly changed median between the groups. These include the VLDL1, VLDL2, and LDL aver-

TABLE 2. The fitted model parameter values for 16 subjects from Packard et al. (29)

Subject	Percentage Deviation	Liver Binding Min Size (nm)	Liver Binding Shape (nm)	ApoE Related Uptake Shape (nm)	ApoB Related Uptake Affinity (day <sup>-1</sup> )	Liver Binding Max Rate (day <sup>-1</sup> )	LPL Related Binding Max Rate (day <sup>-1</sup> )
		$d_{a,apoE \text{ min}}$	$\sigma_{a,apoE}$	$\sigma_{u,apoE}$	$k_{u,apoB}$	$k_{a,apoE \text{ max}}$	$k_{l \text{ max}}$
1	7.1	25.0	199.0	35.2	0.99	467.4	252.9
2	1.6	24.6	30.5	8953.0	0.75	22.0	131.5
3	4.3	25.0	32.5	4160.9	0.45	8.0	107.4
4	12.1	23.7	30.3	2687.4	0.56	2.7	98.5
5	3.2	22.5	199.5	37.6	0.38	96.8	6.5
6	3.6	25.4	28.3	70.5	0.48	79.4	72.6
7	9.6	24.6	33.0	4641.6	0.50	8.3	78.0
8	16.6	25.1	47.0	41.6	0.47	30.4	0.0
9	4.0	24.7	63.3	42.1	0.28	28.1	0.0
11	7.2	24.9	199.8	36.0	0.26	126.9	13.7
12	9.6	25.1	36.9	39.5	0.47	21.6	0.0
14	3.1	23.2	51.0	48.4	0.22	6.2	0.0
17	7.0	21.0	29.4	4097.2	0.38	2.9	42.9
18	15.9	18.6	199.6	38.3	0.29	29.6	18.9
19	4.1	11.0	85.6	39.2	0.24	8.1	26.6
20	6.3	18.8	199.8	39.2	0.29	29.2	7.4
Averages							
A		24.5	73.7	2296.7	0.54	82.6	83.1
I		24.4	95.9	41.3	0.32	51.6	4.6
B		(* ) 17.3	128.6	1053.5	0.30	17.4	24.0
Significance Inter-group Difference							
P		0.014	0.308	0.410	0.034	0.738	0.087

Only subjects with a data set corresponding to steady-state were selected. The patients were grouped by Packard et al. into three phenotype classes, according to their 'LDL peak size'. Class A had a peak size >26 nm, class I between 25 and 26 nm and class B <25 nm. Lower LDL peak size is thought to correspond to a higher risk for cardiovascular disease. The fitted model parameter average for each of these classes is given and the significance of inter-group difference according to the nonparametric Kruskal-Wallis test. An asterisk indicates the group that differs significantly from the other two groups with  $P < 0.05$ .

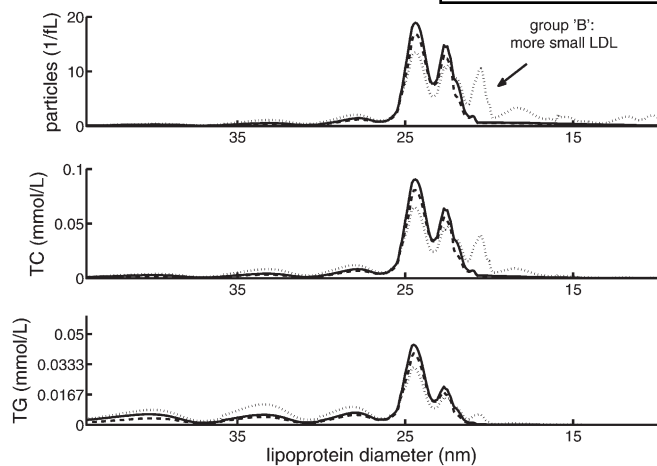


**Fig. 4.** Particle Profiler model results: average particle, total cholesterol (TC) and triglyceride (TG) concentrations of model fits based on flux data of VLDL1, VLDL2, IDL, and LDL only. The three curves represent averages of the subjects in the three phenotype groups as determined by Packard et al. (29). The striped line indicates phenotype A (LDL peak size >26 nm), the solid line phenotype I (LDL peak size between 25 and 26 nm) and the dotted line phenotype B (LDL peak size <25 nm). Although the flux data did not contain any particle size information further than the four mentioned classes, the model results do show more small LDL particles in the class of patients with phenotype B. This corresponds to the LDL size shift measured by Packard et al. and, therefore, gives confidence in the physiological realism of the model.

age particle age; the IDL and LDL average particle size; the VLDL1, VLDL2, and LDL average lipolysis binding rate in general and specifically for HL in VLDL1 and LDL; and the LDL uptake rate.

A similar group-comparison analysis was done based on the flux parameters Packard et al. (29) report in their paper and using the same patients we did. In that case, next to the pool sizes, only the transfer rate of VLDL1 to VLDL2 differs significantly between the groups.

The Particle Profiler model, therefore, seems to be able to sensitively indicate relevant differences in physiology between groups with a differing LDL peak size.

### Simulation of genetic defects

**Figure 5** shows the model fit of patient 20 and simulated defects affecting ApoB-mediated uptake and LPL lipolysis affinity. The cholesterol and triglyceride concentrations in different size classes for the simulated ApoB-mediated uptake reduction show the expected hypercholesterolemia (49). The halved ApoB-related uptake affinity results in a 1.7-fold increase of the LDL-cholesterol concentration in plasma.

The modeled lipolysis affinity reduction also reproduces the expected hypertriglyceridemia (27), although less severely than the hypercholesterolemia induced above. Reducing the LPL lipolysis affinity (by 50%) results in a 1.5-fold increase of VLDL1-triglyceride concentration in plasma. The modeled genetic variants, therefore, qualitatively resemble the observed phenotype.

**TABLE 3.** Derived process indicator parameters for 16 subjects from Packard et al. (29).

Subject	LPL Related Binding Max Rate (day <sup>-1</sup> )	HL Peak Binding Rate (day <sup>-1</sup> )	HL Binding Peak Size (nm)	ApoB Uptake Affinity (day <sup>-1</sup> )	Average ApoE-related Uptake Binding VLDL1 (day <sup>-1</sup> )
1	252.9	27.4	35.2	0.99	91.0
2	131.5	22.0	30.5	0.75	0.7
3	107.4	8.0	32.5	0.45	0.5
4	98.5	2.7	30.3	0.56	0.6
5	6.5	8.2	37.6	0.38	17.8
6	72.6	79.2	28.3	0.48	0.5
7	78.0	8.3	33.0	0.50	0.5
8	0.0	18.3	38.3	0.47	16.8
9	0.0	11.6	40.6	0.28	13.9
11	13.7	8.1	36.0	0.26	23.9
12	0.0	16.7	34.2	0.47	6.5
14	0.0	4.2	41.8	0.22	2.5
17	42.9	2.9	29.4	0.38	0.4
18	18.9	3.2	38.2	0.29	5.6
19	26.6	2.9	37.4	0.24	3.6
20	7.4	3.3	39.1	0.29	5.3
Averages					
A	83.1	20.6	34.0	(*) 0.54	15.8
I	4.6	9.7	37.3	0.32	11.0
B	24.0	(*) 3.1	36.0	0.30	3.7
Significance Inter-group Difference					
P	0.087	0.043	0.512	0.034	0.539

Data and testing as in Table 2.

## DISCUSSION

This study presents Particle Profiler, a model framework capable of analyzing cholesterol and triglyceride data by describing how lipoprotein production, remodeling, and uptake processes depend on lipoprotein particle size. The model was applied to existing preanalyzed stable isotope tracer data presented by Packard et al. (29). Our model implementation was able to reproduce the original model fits by Packard et al., requiring only six parameters to describe all modeled lipolysis and uptake processes. The Particle Profiler results were able to predict the LDL size shift that was measured in the original study, only using reported flux data measured in four density classes by Packard et al. Furthermore, Particle Profiler was able to sensitively indicate relevant differences in physiology between the groups. Finally, the potential for modeling the effects of genetic variants was demonstrated by simulating reductions in ApoB-related uptake affinity and lipolysis affinity.

The biological realism of the Particle Profiler model is largely determined by the correctness of the hypotheses describing how different processes depend on particle size. Although the current set of assumptions reproduces the flux data well, uncertainties still exist. The three datasets that were not fitted well indicate that improvements are needed in the uptake function because the modeled uptake is too high in the IDL and VLDL2 classes. Also, the model for particle triglyceride loss per lipolysis event

TABLE 4. Derived size-specific indicator parameters that showed a significant difference ( $P < 0.05$ ) between groups using the nonparametric Kruskal-Wallis test

	Units	Group Means			Significance Inter-group Difference
		A	I	B	<i>P</i>
Packard-from Published Process Parameters					
Transfer from VLDL1 to VLDL2	(pools/day)	16.8	5.9	5.8	0.0144
Size-specific Process Indicator Parameters					
Average particle lipolysis rate LDL	day <sup>-1</sup>	0.05	0.03	0.55	0.026
Average particle lipolysis rate VLDL2	day <sup>-1</sup>	13.05	8.96	3.37	0.026
Average particle lipolysis rate VLDL1	day <sup>-1</sup>	25.76	7.68	7.77	0.005
Average particle uptake rate LDL	day <sup>-1</sup>	0.54	0.32	0.32	0.042
Average particle HL attachment rate LDL	day <sup>-1</sup>	0.05	0.03	0.55	0.026
Average particle HL attachment rate VLDL2	day <sup>-1</sup>	10.94	8.85	2.77	0.034
Size and Age Parameters					
Average particle age LDL	hours	33.67	59.85	74.65	0.014
Average particle age VLDL2	hours	2.16	3.96	4.91	0.026
Average particle age VLDL1	hours	0.67	1.40	1.62	0.026
Average particle diameter LDL	nm	23.45	23.52	19.22	0.027
Average particle diameter IDL	nm	26.45	26.52	27.35	0.039

Data as in Table 2. When we tested the patients, we selected using variables from the original publication. This showed a difference between groups in one process: transfer from VLDL1 to VLDL2. The current analysis showed five significantly different processes. It indicated lipolysis changes in the LDL, VLDL2, and VLDL1 region, as well as indicating a changed HL activity in the LDL and VLDL2 range. These changes were found to be biologically plausible (see Discussion).

would benefit from more biological underpinning. The data we have analyzed in this paper do not contain enough information to identify this process exactly. We could see that the hypothesis that a particle loses a fixed quantity of triglycerides per lipolysis step is highly unlikely as the corresponding model cannot fit the data. We could not distinguish the possibility that a particle that uses a fixed percentage of triglycerides per lipolysis step from the possibility that a particle loses a stochastic percentage of triglycerides per lipolysis step. Therefore, we have chosen the simplest possible model. Future investigation with more detailed datasets on both particle concentration and particle composition at different particle sizes may allow more insight into this issue. Also, the values for the constants  $d_{\min}$  and  $\sigma_1$  describing how extrahepatic lipolysis depends on particle size require further investigation. The current model framework does provide the structure to investigate these issues.

In order to check the correspondence between our analysis and the original analysis by Packard et al., we can compare the patients' parameter values. A direct comparison is impossible, because the different models have different parameters. However, there should be a qualitative correspondence between the "fractional catabolic rate of LDL" and the "direct catabolism of VLDL1" in Packard's model and the "ApoB-related uptake rate" and the "average ApoE-related uptake binding of VLDL1" in the Particle Profiler model. We can see that in general patients with high or low values for these parameters in Packard's model have high or low values for the corresponding parameters in our model. The qualitative correspondence between similar parameter values in the model by Packard et al. and Particle Profiler is therefore correct.

Our analysis shows a clear difference in several parameters between groups A and B with a measured LDL peak size above 26 nm and under 25 nm, respectively, as defined in (29). The position of the three fitted patients in the intermediate I group with measured LDL peak size between 25 and 26 nm, as defined in (29), is ambiguous in our analysis. The LDL peak size reproduced by our model resembles the A group, but some parameters derived from the model, such as ApoB-related uptake and the LDL and VLDL 1 particle lipolysis rates, resemble the B group. Because of this ambiguity, we will disregard the intermediate

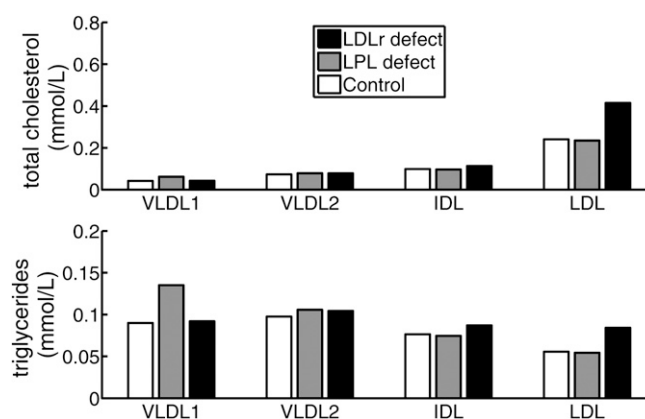


Fig. 5. Total cholesterol (TC) and triglyceride (TG) concentration in model fit for patient 17 (white bars), a simulated lipolysis polymorphism reducing the lipolysis affinity (gray bars), and a simulated ApoB-related uptake polymorphism, reducing the ApoB-related uptake affinity (black bars). The lipolysis polymorphism specifically increases VLDL1 triglycerides. The ApoB-related uptake polymorphism increases LDL cholesterol. Both simulations are in accordance with observed phenotypes.

group and focus on the differences between the A and B groups in continuation.

Comparing our results to those in the original paper by Packard et al. (29), we see that Particle Profiler backs up the statement by Packard, who considers the efficiency of VLDL1 clearance a major controlling factor in small dense LDL formation. Reanalyzing their dataset using Particle Profiler indeed showed a decreased lipolysis affinity in the VLDL1 size range, but also in the VLDL2 size range in patients with smaller LDL. Additionally, in our study, we see that these patients have increased LDL particle lipolysis, a variable that Packard's analysis (29) cannot identify. Therefore, we back up their claim on the relationship between smaller LDL particle size and VLDL1 lipolysis and extend it to VLDL2 and LDL through a more subtle within-class lipolysis analysis. Another additional observation we could make is a decrease in the (ApoB-related) uptake in the LDL range with decreasing particle size.

Therefore, our study identifies several changes in lipoprotein metabolism that are associated with decreased LDL peak size. In agreement with Packard's analysis (29), we find that subjects with decreased LDL peak size have lower LPL lipolysis activity. In addition, we find that HL activity is increased. These findings are in agreement with a study by Campos et al (50). Another study by Tan et al. (51) also finds an increased HL activity when LDL peak size is decreased, but no association with LPL activity. Indeed, HL activity is well known to cause smaller LDL particles (46). What causes the activity of LPL to drop is not clear. Packard et al. (29) indicated that postheparin LPL activity and plasma triglycerides are only weakly correlated and suggested that other factors such as the ApoC-II content or the ApoC-II/C-III ratio in VLDL might determine the lipolysis rate. More recent research has identified additional candidates (40). Finally, our observation that ApoB-related particle uptake decreases with decreasing particle size fits in with earlier studies (52–54). This decrease can be explained by a conformational change in the ApoB molecule on the smaller particles, which results in a less efficient interaction with the LDL receptor (52). We conclude that the processes identified by our analysis as changing with decreasing LDL peak size are biologically plausible.

There are several important ApoB lipoprotein-associated processes that are not yet included in the Particle Profiler model. One is the exchange of triglycerides and cholesteryl esters between VLDL or LDL and HDL particles through the cholesteryl ester transfer protein (55). Incorporation of this process may be an interesting future development. Another candidate is endothelial lipase, although it seems that this enzyme mainly influences HDL metabolism (56). Its influence on ApoB-containing particles needs to be clarified further. These two mechanisms can be incorporated as soon as the relation between lipoprotein size and enzyme activity is clear.

In contrast with earlier modeling approaches (6–26), Particle Profiler is not an explicit multi-compartment model; instead, it specifies the lipoprotein production, remodeling, and uptake processes as continuous functions

of particle size. It then uses these specifications to calculate the particle concentration in size classes that can be freely chosen. Particle Profiler allows the analysis of various hypotheses concerning how the modeled physiological processes vary as a function of lipoprotein size whereas multi-compartment models explicitly model fluxes between measured classes.


The most similar model to Particle Profiler is that of Hübner et al. (57), which also uses a single-particle perspective. Their approach attempts to include all relevant biochemical reactions and then simplify to obtain numerical traceability. In doing so, the emphasis differs from ours. The model of lipoprotein composition is more detailed with cholesterol and triglyceride content as well as a simplified apolipoprotein content explicitly modeled. The Hübner et al. model also includes HDL and associated processes such as cholesteryl ester transfer protein activity. This model aims to include as much biochemical detail as possible. In contrast, our model focuses on integrated physiological process rates and how these rates depend on the size of the particle. For example, whereas in the Hübner et al. model ApoB-containing particles are produced at a single size, our model includes the full range of production sizes measured in the study we use for validation (29). Starting from integrated physiological rates, Particle Profiler also allows zooming in on biochemical processes that appear to be important. In this way, we introduced the distinction between LPL and HL lipolysis of ApoB-containing lipoproteins, a distinction that Hübner et al. do not make. In the present study, the distinction was important because these two enzymes showed a different response to changing LDL peak size.

The advantage of Particle Profiler over earlier multi-compartment models is two-fold. First, it can analyze and reproduce more detailed lipoprotein size profiles. The detailed calculation is important, because the output can then be given in any set of size classes required, such as those corresponding to the classical VLDL, IDL, and LDL fractionation but equally well for HPLC (27) and NMR (28) measurements. These different types of data can all be analyzed using our model framework. To actually start using these types of data for model optimization will require an independent estimate of the production fluxes as input to the model. This is due to the fact that data from an HPLC or NMR measurement does not contain the production flux information the study by Packard et al. (29) provides. Lipoprotein profile data alone are therefore insufficient to fit the production fluxes. Methods to determine production fluxes include stable isotope methods [see (58) for a review], Intralipid (59), and estimation based on other plasma biomarkers [e.g., see (60)]. Together with independent production estimates, data from detailed lipoprotein size profiles suffice to calculate lipolysis and uptake through different mechanisms.

The second advantage of Particle Profiler above multi-compartment models is its more direct link with the physiology of individual lipoprotein particles. The model analysis leads to 'integrated physiological process rates' of processes affecting lipoprotein particles. It is important to



note that enzymes other than those identified and incorporated into the model may contribute to determining these rates. Still, the integrated process rates are a step closer to actual enzyme activities than the fluxes between classes reported by earlier models. For example, the affinity of a VLDL1 particle for the lipolysis process gives more information about LPL and HL activity than the ApoB transfer rate from VLDL1 to VLDL2. At the same time, the integrated process rates are one organization level higher than the enzyme activities used by Hübner et al. (57). This means the description can be simpler. A simpler description in turn leads to fewer parameters to be estimated and, therefore, less data is needed for parameter estimation. In this way, Particle Profiler finds an efficient balance between the need for biological insight and the practical identifiability of model parameters based on available data.

Particle Profiler can calculate rates of various lipoprotein lipolysis and uptake processes from detailed lipoprotein size measurements and an independent production estimate. This information will be useful for diagnostic purposes. 

The authors gratefully acknowledge the helpful comments of our two anonymous referees.

## REFERENCES

1. Grundy, S. M. 2004. Richard Havel, Howard Eder, and the evolution of lipoprotein analysis. *J. Clin. Invest.* **114**: 1034–1037.
2. Austin, M. A., M. C. King, K. M. Vranizan, and R. M. Krauss. 1990. Atherogenic lipoprotein phenotype. A proposed genetic marker for coronary heart disease risk. *Circulation*. **82**: 495–506.
3. Alaupovic, P. 1991. Apolipoprotein composition as the basis for classifying plasma lipoproteins: characterization of ApoA- and ApoB-containing lipoprotein families. *Prog. Lipid Res.* **30**: 105–138.
4. Alaupovic, P. 1996. Significance of apolipoproteins for structure, function, and classification of plasma lipoproteins. *Methods Enzymol.* **263**: 32–60.
5. Walldius, G., A. H. Aastveit, and I. Jungner. 2006. Stroke mortality and the apoB/apoA-I ratio: results of the AMORIS prospective study. *J. Intern. Med.* **259**: 259–266.
6. Phair, R. D., M. G. Hammond, J. A. Bowden, M. Fried, W. R. Fisher, and M. Berman. 1975. Preliminary model for human lipoprotein metabolism in hyperlipoproteinemia. *Fed. Proc.* **34**: 2263–2270.
7. Berman, M., M. Hall III, R. I. Levy, S. Eisenberg, D. W. Bilheimer, R. D. Phair, and R. H. Goebel. 1978. Metabolism of apoB and apoC lipoproteins in man: kinetic studies in normal and hyperlipoproteinemic subjects. *J. Lipid Res.* **19**: 38–56.
8. Fisher, W. R., L. A. Zech, P. Bardalaye, G. Warmke, and M. Berman. 1980. The metabolism of apolipoprotein B in subjects with hypertriglyceridemia and polydisperse LDL. *J. Lipid Res.* **21**: 760–774.
9. Beltz, W. F., Y. A. Kesaniemi, B. V. Howard, and S. M. Grundy. 1985. Development of an integrated model for analysis of the kinetics of apolipoprotein B in plasma very low density lipoproteins, intermediate density lipoproteins, and low density lipoproteins. *J. Clin. Invest.* **76**: 575–585.
10. Fisher, W. R., L. A. Zech, L. L. Kilgore, and P. W. Stacpoole. 1991. Metabolic pathways of apolipoprotein B in heterozygous familial hypercholesterolemia: studies with a [<sup>3</sup>H]leucine tracer. *J. Lipid Res.* **32**: 1823–1836.
11. Packard, C. J., A. Munro, A. R. Lorimer, A. M. Gotto, and J. Shepherd. 1984. Metabolism of apolipoprotein B in large triglyceride-rich very low density lipoproteins of normal and hypertriglyceridemic subjects. *J. Clin. Invest.* **74**: 2178–2192.

12. Ginsberg, H. N., N. A. Le, and J. C. Gibson. 1985. Regulation of the production and catabolism of plasma low density lipoproteins in hypertriglyceridemic subjects. Effect of weight loss. *J. Clin. Invest.* **75**: 614–623.
13. Krul, E. S., K. G. Parhofer, P. H. Barrett, R. D. Wagner, and G. Schonfeld. 1992. ApoB-75, a truncation of apolipoprotein B associated with familial hypobetalipoproteinemia: genetic and kinetic studies. *J. Lipid Res.* **33**: 1037–1050.
14. Packard, C. J., A. Gaw, T. Demant, and J. Shepherd. 1995. Development and application of a multicompartmental model to study very low density lipoprotein subfraction metabolism. *J. Lipid Res.* **36**: 172–187.
15. Malmstrom, R., C. J. Packard, T. D. Watson, S. Rannikko, M. Caslake, D. Bedford, P. Stewart, H. Yki-Jarvinen, J. Shepherd, and M. R. Taskinen. 1997. Metabolic basis of hypotriglyceridemic effects of insulin in normal men. *Arterioscler. Thromb. Vasc. Biol.* **17**: 1454–1464.
16. Patterson, B. W., B. Mittendorfer, N. Elias, R. Satyanarayana, and S. Klein. 2002. Use of stable isotopically labeled tracers to measure very low density lipoprotein-triglyceride turnover. *J. Lipid Res.* **43**: 223–233.
17. Zech, L. A., S. M. Grundy, D. Steinberg, and M. Berman. 1979. Kinetic model for production and metabolism of very low density lipoprotein triglycerides. Evidence for a slow production pathway and results for normolipidemic subjects. *J. Clin. Invest.* **63**: 1262–1273.
18. Melish, J., N. A. Le, H. Ginsberg, D. Steinberg, and W. V. Brown. 1980. Dissociation of apoprotein B and triglyceride production in very-low-density lipoproteins. *Am. J. Physiol.* **239**: E354–E362.
19. Harris, W. S., W. E. Connor, D. R. Illingworth, D. W. Rothrock, and D. M. Foster. 1990. Effects of fish oil on VLDL triglyceride kinetics in humans. *J. Lipid Res.* **31**: 1549–1558.
20. Barrett, P. H., N. Baker, and P. J. Nestel. 1991. Model development to describe the heterogeneous kinetics of apolipoprotein B and triglyceride in hypertriglyceridemic subjects. *J. Lipid Res.* **32**: 743–762.
21. Adiels, M., C. Packard, M. J. Caslake, P. Stewart, A. Soro, J. Westerbacka, B. Wennberg, S. O. Olofsson, M. R. Taskinen, and J. Borén. 2005. A new combined multicompartmental model for apolipoprotein B-100 and triglyceride metabolism in VLDL subfractions. *J. Lipid Res.* **46**: 58–67.
22. Campos, H., D. Perlov, C. Khoo, and F. M. Sacks. 2001. Distinct patterns of lipoproteins with apoB defined by presence of apoE or apoC-III in hypercholesterolemia and hypertriglyceridemia. *J. Lipid Res.* **42**: 1239–1249.
23. Tomiyasu, K., B. W. Walsh, K. Ikewaki, H. Judge, and F. M. Sacks. 2001. Differential metabolism of human VLDL according to content of apoE and apoC-III. *Arterioscler. Thromb. Vasc. Biol.* **21**: 1494–1500.
24. Zheng, C., C. Khoo, K. Ikewaki, and F. M. Sacks. 2007. Rapid turnover of apolipoprotein C-III-containing triglyceride-rich lipoproteins contributing to the formation of LDL subfractions. *J. Lipid Res.* **48**: 1190–1203.
25. Chan, D. C., G. F. Watts, M. N. Nguyen, and P. H. Barrett. 2006. Apolipoproteins C-III and A-V as predictors of very-low-density lipoprotein triglyceride and apolipoprotein B-100 kinetics. *Arterioscler. Thromb. Vasc. Biol.* **26**: 590–596.
26. Cohn, J. S., B. W. Patterson, K. D. Uffelman, J. Davignon, and G. Steiner. 2004. Rate of production of plasma and very-low-density lipoprotein (VLDL) apolipoprotein C-III is strongly related to the concentration and level of production of VLDL triglyceride in male subjects with different body weights and levels of insulin sensitivity. *J. Clin. Endocrinol. Metab.* **89**: 3949–3955.
27. Okazaki, M., S. Usui, M. Ishigami, N. Sakai, T. Nakamura, Y. Matsuzawa, and S. Yamashita. 2005. Identification of unique lipoprotein subclasses for visceral obesity by component analysis of cholesterol profile in high-performance liquid chromatography. *Arterioscler. Thromb. Vasc. Biol.* **25**: 578–584.
28. Otvos, J. D., E. J. Jeyarajah, D. W. Bennett, and R. M. Krauss. 1992. Development of a proton nuclear magnetic resonance spectroscopic method for determining plasma lipoprotein concentrations and subspecies distributions from a single, rapid measurement. *Clin. Chem.* **38**: 1632–1638.
29. Packard, C. J., T. Demant, J. P. Stewart, D. Bedford, M. J. Caslake, G. Schwartzfeger, A. Bedynek, J. Shepherd, and D. Seidel. 2000. Apolipoprotein B metabolism and the distribution of VLDL and LDL subfractions. *J. Lipid Res.* **41**: 305–318.

30. Blasiolo, D. A., R. A. Davis, and A. D. Attie. 2007. The physiological and molecular regulation of lipoprotein assembly and secretion. *Mol. Biosyst.* **3**: 608–619.
31. Stillemark-Billton, P., C. Beck, J. Borén, and S. O. Olofsson. 2005. Relation of the size and intracellular sorting of apoB to the formation of VLDL 1 and VLDL 2. *J. Lipid Res.* **46**: 104–114.
32. Olofsson, S. O., and J. Borén. 2005. Apolipoprotein B: a clinically important apolipoprotein which assembles atherogenic lipoproteins and promotes the development of atherosclerosis. *J. Intern. Med.* **258**: 395–410.
33. Olofsson, S. O., P. Boström, L. Andersson, M. Rutberg, J. Perman, and J. Borén. 2008. Lipid droplets as dynamic organelles connecting storage and efflux of lipids. *Biochim. Biophys. Acta.* **1791**: 448–458.
34. Tuzikov, F. V., N. A. Tuzikova, R. V. Galimov, L. E. Panin, and G. A. Nevinsky. 2002. General model to describe the structure and dynamic balance between different human serum lipoproteins and its practical application. *Med. Sci. Monit.* **8**: MT79–MT88.
35. Lichtenstein, L., J. F. Berbee, S. J. van Dijk, K. W. Van Dijk, A. Bensadoun, I. P. Kema, P. J. Voshol, M. Muller, P. C. Rensen, and S. Kersten. 2007. Angptl4 upregulates cholesterol synthesis in liver via inhibition of LPL- and HL-dependent hepatic cholesterol uptake. *Arterioscler. Thromb. Vasc. Biol.* **27**: 2420–2427.
36. Demant, T., A. Gaw, G. F. Watts, P. Durrington, B. Buckley, C. W. Imrie, C. Wilson, C. J. Packard, and J. Shepherd. 1993. Metabolism of apoB-100-containing lipoproteins in familial hyperchylomicronemia. *J. Lipid Res.* **34**: 147–156.
37. Young, S. G., B. S. Davies, L. G. Fong, P. Gin, M. M. Weinstein, A. Bensadoun, and A. P. Beigneux. 2007. GPIHBP1: an endothelial cell molecule important for the lipolytic processing of chylomicrons. *Curr. Opin. Lipidol.* **18**: 389–396.
38. de Beer, F., W. L. Hendriks, L. C. van Vark, S. W. A. Kamerling, K. W. van Dijk, M. H. Hofker, A. H. M. Smelt, and L. M. Havekes. 1999. Binding of beta-VLDL to heparan sulfate proteoglycans requires lipoprotein lipase, whereas ApoE only modulates binding affinity. *Arterioscler. Thromb. Vasc. Biol.* **19**: 633–637.
39. Adiels, M. 2004. *Compartmental Models of Lipoprotein Kinetics*. PhD Thesis, Chalmers University of Technology, Göteborg, Sweden.
40. Voshol, P. J., P. C. Rensen, K. W. Van Dijk, J. A. Romijn, and L. M. Havekes. 2009. Effect of plasma triglyceride metabolism on lipid storage in adipose tissue: studies using genetically engineered mouse models. *Biochim. Biophys. Acta.* **1791**: 479–485.
41. Demant, T., L. A. Carlson, L. Holmquist, F. Karpe, P. Nilsson-Ehle, C. J. Packard, and J. Shepherd. 1988. Lipoprotein metabolism in hepatic lipase deficiency: studies on the turnover of apolipoprotein B and on the effect of hepatic lipase on high density lipoprotein. *J. Lipid Res.* **29**: 1603–1611.
42. Krieger, M. 1994. Structures and functions of multiligand lipoprotein receptors: macrophage scavenger receptors and LDL receptor-related protein (LRP). *Annu. Rev. Biochem.* **63**: 601–637.
43. MacArthur, J. M., J. R. Bishop, K. I. Stanford, L. C. Wang, A. Bensadoun, J. L. Witztum, and J. D. Esko. 2007. Liver heparan sulfate proteoglycans mediate clearance of triglyceride-rich lipoproteins independently of LDL receptor family members. *J. Clin. Invest.* **117**: 153–164.
44. Van Eck, M., M. Hoekstra, R. Out, I. S. Bos, J. K. Kruijt, R. B. Hildebrand, and T. J. van Berkel. 2008. Scavenger receptor BI facilitates the metabolism of VLDL lipoproteins in vivo. *J. Lipid Res.* **49**: 136–146.
45. Stein, Y., and O. Stein. 2003. Lipoprotein lipase and atherosclerosis. *Atherosclerosis.* **170**: 1–9.
46. Zamboni, A., S. S. Deeb, P. Pauletto, G. Crepaldi, and J. D. Brunzell. 2003. Hepatic lipase: a marker for cardiovascular disease risk and response to therapy. *Curr. Opin. Lipidol.* **14**: 179–189.
47. Connelly, P. W., G. F. Maguire, C. Vezina, R. A. Hegele, and A. Kuksis. 1994. Kinetics of lipolysis of very low density lipoproteins by lipoprotein lipase. Importance of particle number and noncompetitive inhibition by particles with low triglyceride content. *J. Biol. Chem.* **269**: 20554–20560.
48. Schreier, L., G. Berg, V. Zago, A. I. Gonzalez, and R. Wikinski. 2002. Kinetics of in vitro lipolysis of human very low-density lipoprotein by lipoprotein lipase. *Nutr. Metab. Cardiovasc. Dis.* **12**: 13–18.
49. Guerin, M., P. J. Dolphin, C. Talussot, J. Gardette, F. Berthezene, and M. J. Chapman. 1995. Pravastatin modulates cholesteryl ester transfer from HDL to ApoB-containing lipoproteins and lipoprotein subspecies profile in familial hypercholesterolemia. *Arterioscler. Thromb. Vasc. Biol.* **15**: 1359–1368.
50. Campos, H., D. M. Dreon, and R. M. Krauss. 1995. Associations of hepatic and lipoprotein lipase activities with changes in dietary composition and low density lipoprotein subclasses. *J. Lipid Res.* **36**: 462–472.
51. Tan, C. E., L. Forster, M. J. Caslake, D. Bedford, T. D. G. Watson, M. McConnell, C. J. Packard, and J. Shepherd. 1995. Relations between plasma lipids and postheparin plasma lipases and VLDL and LDL subfraction patterns in normolipemic men and women. *Arterioscler. Thromb. Vasc. Biol.* **15**: 1839–1848.
52. Chen, G. C., W. Liu, P. Duchateau, J. Allaart, R. L. Hamilton, C. M. Mendel, K. Lau, D. A. Hardman, P. H. Frost, and M. J. Malloy. 1994. Conformational differences in human apolipoprotein B-100 among subspecies of low density lipoproteins (LDL). Association of altered proteolytic accessibility with decreased receptor binding of LDL subspecies from hypertriglyceridemic subjects. *J. Biol. Chem.* **269**: 29121–29128.
53. Nigon, F., P. Lesnik, M. Rouis, and M. J. Chapman. 1991. Discrete subspecies of human low density lipoproteins are heterogeneous in their interaction with the cellular LDL receptor. *J. Lipid Res.* **32**: 1741–1753.
54. Campos, H., K. S. Arnold, M. E. Balestra, T. L. Innerarity, and R. M. Krauss. 1996. Differences in receptor binding of LDL subfractions. *Arterioscler. Thromb. Vasc. Biol.* **16**: 794–801.
55. Thompson, A., E. Di Angelantonio, N. Sarwar, S. Erqou, D. Saleheen, R. P. F. Dullaart, B. Keavney, Z. Ye, and J. Danesh. 2008. Association of cholesteryl ester transfer protein genotypes with CETP mass and activity, lipid levels, and coronary risk. *JAMA.* **299**: 2777–2788.
56. Lamarche, B., and M. E. Paradis. 2007. Endothelial lipase and the metabolic syndrome. *Curr. Opin. Lipidol.* **18**: 298–303.
57. Hubner, K., T. Schwager, K. Winkler, J. G. Reich, and H. G. Holzhauser. 2008. Computational lipidology: predicting lipoprotein density profiles in human blood plasma. *PLOS Comput. Biol.* **4**: e1000079.
58. Magkos, F., and L. S. Sidossis. 2004. Measuring very low density lipoprotein-triglyceride kinetics in man in vivo: how different the various methods really are. *Curr. Opin. Clin. Nutr. Metab. Care.* **7**: 547–555.
59. Al-Shayji, I. A. R., J. M. R. Gill, J. Cooney, S. Siddiqui, and M. J. Caslake. 2007. Development of a novel method to determine very low density lipoprotein kinetics. *J. Lipid Res.* **48**: 2086–2095.
60. Adiels, M., M. R. Taskinen, C. Packard, M. J. Caslake, A. Sorva, J. Westerbacka, S. Vehkavaara, A. Häkkinen, S. O. Olofsson, H. Yki-Järvinen, and J. Borén. 2006. Overproduction of large VLDL particles is driven by increased liver fat content in man. *Diabetologia.* **49**: 755–765.